Modeling the Transient Structure of Non-Reacting and Reacting Diesel Sprays

C. Bajaj, M. Ameen, J. Abraham*
School of Mechanical Engineering, Purdue University, West Lafayette, IN 47906-2088, USA
bajajc@purdue.edu, mameen@purdue.edu and jabraham@purdue.edu

Abstract

Modeling the transient structure of reacting diesel sprays accurately is important within the context of multi-dimensional modeling of flows, sprays, and combustion in diesel engines. In the case of non-reacting vaporizing sprays, vapor jets have been shown to reproduce, with adequate accuracy, the structure of the diesel jet beyond the maximum liquid length of about 100 orifice diameters in high-pressure injection into high-pressure high-temperature environments. In this work, the primary focus is on reacting diesel jets. An unsteady flamelet progress variable (UFPV) model for reacting diesel jets is evaluated. The UFPV model has been proposed for predicting the averaged/filtered chemistry source terms in Reynolds averaged simulations (RANS) and large eddy simulations of turbulent non-premixed combustion. In the model, a look-up table of reaction source terms is generated as a function of mixture fraction Z, stoichiometric scalar dissipation rate χ_{st}, and progress variable C_{st} by solving the unsteady flamelet equations. The formulation assumes that the shape of the $\chi(Z)$ profile can be modeled by an error function which remains unchanged in the presence of heat release. It is also assumed that the probability density functions (pdfs) of Z, χ_{st}, and C_{st} are statistically independent, and presumed functions are employed for the pdfs. Changes in injection pressure, ambient temperature, ambient density, orifice diameter, and ambient O_2 concentration are considered. It is shown that the model is able to predict ignition delay and flame lift-off with reasonable accuracy for all conditions. The ability of the model to predict the lift-off height appears to be related to the mechanism by which the flame propagates from the ignition location to the final stabilization plane along the stoichiometric surface.

Introduction

Accurately predicting the spray structure, autoignition, flame development, and flame lift-off in multidimensional modeling of diesel sprays is important to predict heat release rates and pollutant formation accurately. The focus of this work is primarily on the predictions of autoignition, flame development, and flame lift-off, but a brief discussion about the modeling of non-reacting sprays is given below. In conventional diesel engines, where high-pressure injection of the liquid fuel is into high-pressure high-temperature chamber gas, it has been shown that the liquid phase (drops and any continuous liquid core if it exists) penetrates to a distance of about 100 orifice diameters whereas the overall jet penetration is typically an order of magnitude larger [1, 2]. It has also been shown that the structure of the jet is primarily momentum-controlled and the spray can be well-represented by a vapor jet injected with the same mass and momentum flow rates as the spray [3-7].

Figure 1 shows a measured image of a non-reacting vaporizing spray (a), and the computed images of vapor jet (b) and vaporizing spray (c), injected with the same mass and momentum flow rates as the measured spray, at 1.13 ms after start of injection (ASI) [7]. An axisymmetric multidimensional RANS code that has been widely employed in prior work was used [5, 7]. Table 1 lists the measured and computed conditions. The measured images show ensemble-averaged two-dimensional Rayleigh-scattering images [8]. The field of view shown for the computed images is the same as for the measured image. The colors identify concentrations of fuel vapor fraction. The penetration, spreading, and distribution of vapor fuel predicted are about the same. Quantitative comparisons of vapor distribution in the jets beyond the maximum penetration of the liquid phase (about 9 mm in this case) show agreement within about 20% [7]. The computations of Fig. 1(b) were carried out without directly accounting for the vaporization effects on temperature and density in the vapor jet. Recent work [9] has shown that this effect is negligible beyond the first 100 diameters. A virtual-liquid source model has been proposed in the literature [10] which includes the vaporization effects and it has been shown in Ref. [7] to give predictions comparable to that of Fig. 1 (b). It is possible to employ a spray model and get a result comparable to that in Fig. 1 (b) provided an appropriate drop size, which results in rapid momentum transfer and in mixing-controlled vaporization, is selected [2]. Figure 1 (c) shows a simulation employing a Lagrangian-drop model in which the drops have a Sauter-mean diameter of 2 μm. Increasing the size increases the differences between the measured (Fig. 1 (a)) and computed sprays. In spray models, this size is usually determined from atomization sub-models

* Corresponding author: jabraham@purdue.edu

which are the still the subject of inquiry [11-13]. Furthermore, grid independent results are difficult to achieve with the Lagrangian drop model as discussed in the literature [5, 7, 14-16]. For the computations with the spray model above, the grid size stretches in the radial direction from about 0.3 mm at the injector to 2 mm at the wall. Note that the smallest grid is about a factor of 3 larger than the nozzle diameter. Using even smaller grids violates the assumptions of the spray model and leads to computational instabilities. In the axial direction, the grid stretches from about 0.25 mm at the injector to 4.5 mm. For the vapor jet simulations, the grid stretches from a value equal to the nozzle radius or smaller to 4.5 mm in the radial direction and about 0.25 to 4.5 mm in the axial direction. Figure 2 shows comparisons between the (a) penetrations and (b) half-widths of the computed vapor jet and spray [9]. The spray penetrates somewhat farther and its half-width is lower. These quantitative differences can, however, be misleading because the Lagrangian-drop spray simulations are not necessarily grid independent.

Table 1: Experimental and computational conditions

	Spray	Vapor jet
Ambient temperature (K)	1000	1000
Ambient density (kg/m^3)	14.8	14.8
Injected fluid	n-heptane	n-heptane
Density of injected fuel (kg/m^3)	630	136.9
Injection velocity (m/s)	632.4	632.4
Injected fluid temperature (K)	373	373
Orifice diameter (mm)	0.0927	0.199

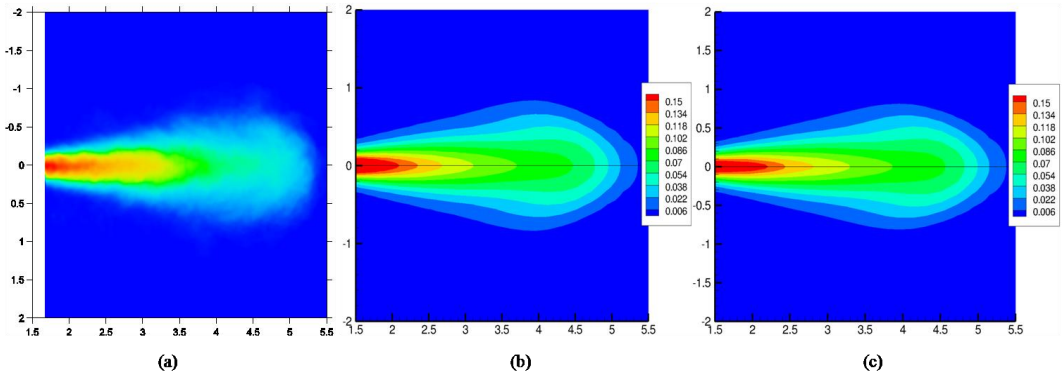

Figure 1. Measured (a), and computed vapor fraction (b,c) contours at 1.13 ms ASI; (b) is with vapor jet and (c) is with liquid spray. Color legend identifies values of vapor fraction [7].

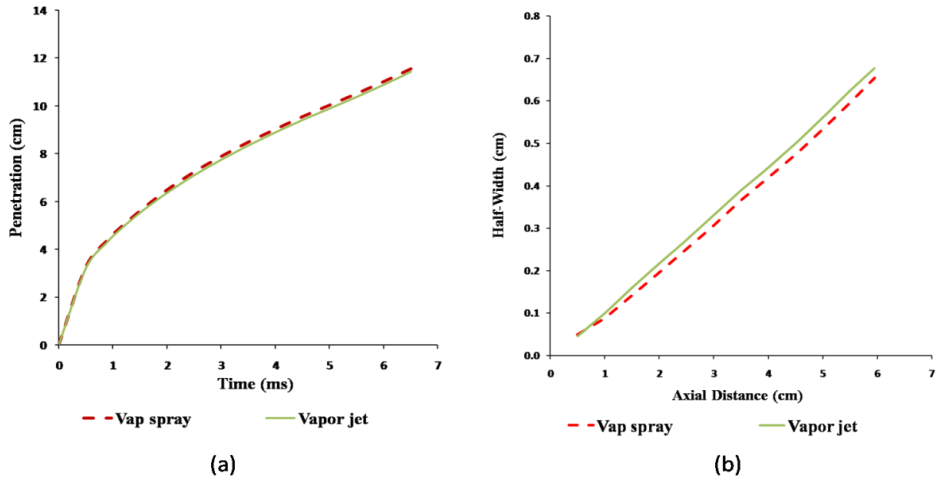

Figure 2. (a) Penetrations and (b) half-widths of the computed vapor jet and spray [9].

Consider next reacting diesel jets. Imaging of flames in diesel jets suggest that reactions occur in relatively thin layers [17]. While the thickness of these layers has not been measured and their detailed structure has not been characterized through measurements in engines, a reasonable assumption is that the layers are laminar non-premixed flames whose structure is influenced by the local turbulence [11, 18-20]. The structure of the flame can be assumed to be that of a strained laminar flamelet [20-22]. Within the context of RANS (or large-eddy) simula-

tions, these effects cannot be directly captured because the reaction and strain occur on scales that are smaller than the grid size. Hence, a turbulence/chemistry interaction model is essential to capture the physical and chemical processes [23, 24]. Successful predictions of autoignition in diesel jets have been shown in prior work by employing kinetic models of varying levels of complexity [25-32]. In many cases, such models are employed without directly taking into account turbulence/chemistry interactions whereas a limited number of studies have taken into account such interactions [27, 29, 31, 32]. Predicting flame lift-off is important because fuel/air mixing upstream of the lift-off height has a controlling effect on soot formation in the jet [33]. In fact, the capability of a model to predict lift-off accurately is a good measure of the accuracy of the overall predictive model. Unfortunately, the flame stabilization mechanism at the lift-off height is not well-understood and several theories have been proposed in the literature to explain it [20, 34-36]. Prior studies exist in the literature. These include the use of a partially stirred reactor model [27, 29, 32], perfectly-stirred reactor (PSR) model [30], a generalized flame surface density (GFSD) model [37], a diffusion flamelet extinction model [31], the representative interactive flamelet approach [38] of Pitsch *et al.* [39] and eddy dissipation and PSR models [40]. In all cases, reasonable agreement with measured results has been reported. This is noteworthy given the significant differences in the models and their assumptions.

In the rest of this paper, a model that can potentially predict ignition, flame development, and flame lift-off over a broad range of conditions, include turbulence-chemistry interactions, but at the same time is computationally inexpensive, is evaluated for reacting diesel jets. Being able to predict autoignition accurately is important because flame lift-off in diesel jets has been suggested to relate to ignition in the jets [41]. Modeling turbulence/chemistry interactions are important in the predictions of both autoignition and flame lift-off. The unsteady flamelet model is suited for representing both multistep kinetics and turbulence-chemistry interactions. More importantly, it is consistent with the structure of reacting diesel jets. The model will be briefly described below, followed by presentation of the results and their discussion. The paper will end with summary and conclusions.

The Computational Model

The same RANS code employed for the non-reacting simulations discussed above will be employed here. Turbulence is modeled with the standard k-ε model and wall functions are employed to model boundary layers [7, 14]. It is well known that the k-e models over-predict the spreading rate of round jets by about 20- 30 % [42, 43]. Corrections to the k-ε model have been proposed to address this limitation in round non-reacting jets [44] but the correction is not universal, and can lead to other difficulties and errors in other flow situations. Hence, the correction is rarely employed in engine simulations.

The unsteady flamelet progress variable (UFPV) model evaluated in this work was presented in prior work [45, 46]. In the model, the chemical source terms obtained by solving the unsteady flamelet equations are tabulated in a look-up table as a function of three independent parameters: the mixture fraction Z, and the progress variable C_{st} and the scalar dissipation rate χ_{st} estimated at the stoichiometric mixture fraction (denoted by '*st*'). The unsteady flamelet equations can be written as [21]

$$\dot{\varphi} = \frac{\chi}{2}\frac{\partial^2 \varphi}{\partial Z^2} + \dot{\omega}_{\varphi}, \tag{1}$$

where φ is a vector that represents the collective set of all reactive scalars, i.e. temperature and species mass fractions, $\dot{\varphi}$ is the rate of change of the reactive scalar, $\dot{\omega}_{\varphi}$ represents the source terms, and χ is the instantaneous scalar dissipation rate defined as

$$\chi = 2D\left|\nabla Z\right|^2, \tag{2}$$

where D is the molecular diffusivity. The functional form of the dependence of χ on Z is typically given by an error function profile [21]

$$\chi = \chi_{st}\frac{\exp\left\{-2\left[erfc^{-1}\left(2Z\right)\right]^2\right\}}{\exp\left\{-2\left[erfc^{-1}\left(2Z_{st}\right)\right]^2\right\}}. \tag{3}$$

The solution of Eq. (1), with boundary conditions representing the conditions in the fuel and air streams and initial conditions representing the unburned state of the mixture, for a specified value of χ_{st}, provides the transient solution for the source terms. The measured results with which computed results are compared in this work were obtained in a constant-volume chamber where the pressure was approximately constant. For this reason, the assumption is made that the pressure is constant in the solution. The transient solutions can be obtained for a range of values of χ_{st} that are representative of the χ_{st} values encountered in the jet. Once the solutions are obtained, they are tabulated as a function of independent variables and employed in the simulations of the reacting diesel jet, as described below. The choice of independent variables will be discussed next.

One obvious independent variable is the mixture fraction Z. The other is the stoichiometric value of scalar dissipation rate χ_{st}. Note that $\chi(Z)$ is characterized in Eq. (3) for a given value of χ_{st}. A third variable C is a measure of the progress of reaction, defined in this work on the basis of a normalized rise in temperature as

$$C = \frac{T - T_u}{T_a - T_u}, \tag{4}$$

where T is the temperature at a time instant at a certain value of Z, and the subscripts 'a' and 'u' indicate adiabatic and unburned conditions, respectively. In general, C is a function of Z. To simplify the look-up table, the assumption is made that the C(Z) profile can be characterized by the stoichiometric value of C, i.e. C_{st}. This profile is obtained from a separate look-up table where C(Z) is tabulated for different values of C_{st} during the transient evolution of the flamelet. There is an implicit assumption that given a value of C_{st}, the C at any Z is unique. Ref. [47] has shown that this is a reasonable assumption. This is analogous to the treatment of χ(Z) in Eq. (3). Note that C(Z) values can be obtained for both igniting and extinguishing flames [45, 46]. In RANS simulations, the average source terms are required. These can be obtaining by convolving the instantaneous source terms in the look-up table with the joint probability density function (PDF), $\tilde{P}\left(Z, C_{st}, \chi_{st}\right)$, of the independent variables, i.e.

$$\tilde{\omega}_{\varphi} = \iiint \dot{\varphi} \tilde{P}\left(Z, C_{st}, \chi_{st}\right) dZ dC_{st} d\chi_{st}, \tag{5}$$

where ~ denotes Fávre averaging. In the UFPV implementation reported in the literature, the assumption is made that the PDFs of the independent variables are statistically independent of each other [45, 46]. This assumption has also been assessed in detail in Ref. [47]. Statistical independence converts the conditional PDFs into their respective marginal PDFs, i.e.

$$\tilde{P}\left(Z, C_{st}, \chi_{st}\right) = \tilde{P}\left(Z\right)\tilde{P}\left(C_{st}\right)\tilde{P}\left(\chi_{st}\right). \tag{6}$$

Presumed functional forms will be employed to approximate the shapes of the PDFs of the three variables Z, C_{st} and χ_{st}. The β-PDF is employed for Z and δ-PDFs for C_{st} and χ_{st}.

Results and Discussion

The measured values of ignition delay and lift-off height were obtained in a constant-volume chamber and they are available on the Engine Combustion Network maintained by Sandia National Laboratories, Livermore, CA (http://www.ca.sandia.gov/ECN). n-Heptane was employed as the fuel. In addition to solving the governing equations of transient reacting flows, transient equations for mixture fraction Z and the variance of the mixture fraction ($Z^{"2}$) are solved. The instantaneous *average* value of scalar dissipation rate $\tilde{\chi}$ in a computational cell is obtained from the RANS simulations as [38, 48]

$$\tilde{\chi} = C_{\chi} \frac{\varepsilon}{k} Z^{"2}. \tag{7}$$

The constant C_{χ} is selected to have a value of 6.5 [38]. A skeletal mechanism for n-heptane oxidation consisting of 44-species and 185 reactions is employed to represent the kinetics [49].

Table 2 lists nine cases simulated in this work. These cases represent changes in injection pressure, orifice diameter and chamber temperature, density and oxygen mass fraction. The d_{noz} parameter in the table represents the nominal nozzle diameter, whereas d_{gas} is the equivalent nozzle diameter when the fuel is injected as a vapor jet instead of as a liquid spray jet.

Table 2. Computational Conditions

Case	d_{noz} (mm)	d_{gas} (mm)	P_{inj} (MPa)	P_{amb} (bar)	T_{fuel} (K)	$T_{ambient}$ (K)	$\rho_{ambient}$ (kg/m^3)	O_2%
1	0.1	0.199	150	42.66	373	1000	14.8	21
2	0.1	0.199	60	42.66	373	1000	14.8	21
3	0.1	0.1745	150	55.45	373	1300	14.8	21
4	0.1	0.2907	150	38.39	373	900	14.8	21
5	0.1	0.199	150	43.02	373	1000	14.8	15
6	0.1	0.199	150	43.2	373	1000	14.8	12
7	0.1	0.199	150	43.45	373	1000	14.8	8
8	0.18	0.3858	140	42.66	373	1000	14.8	21
9	0.1	0.1397	150	86.47	373	1000	30.0	15

While it is not possible to confirm that Lagrangian-drop simulations are grid-independent, it is interesting to compare reacting vapor jet and liquid jet simulations, with the UFPV model, when the highest possible grid resolution (see Fig. 1 (c)) is employed for the spray. Figure 3 shows the temperature contour plots for Cases 1, 3 and 5 of Table 2 at 2.5 ms after start of injection (ASI), when the fuel is injected as a vapor jet (denoted by g in figure) and a liquid spray (denoted by s in figure). The computed lift-off height in the spray case is higher than the corresponding vapor jet. Differences observed between the two may be attributed to the lack of adequate spatial resolution in the spray simulation although there is no way to confirm this. It is encouraging that the results are not very different.

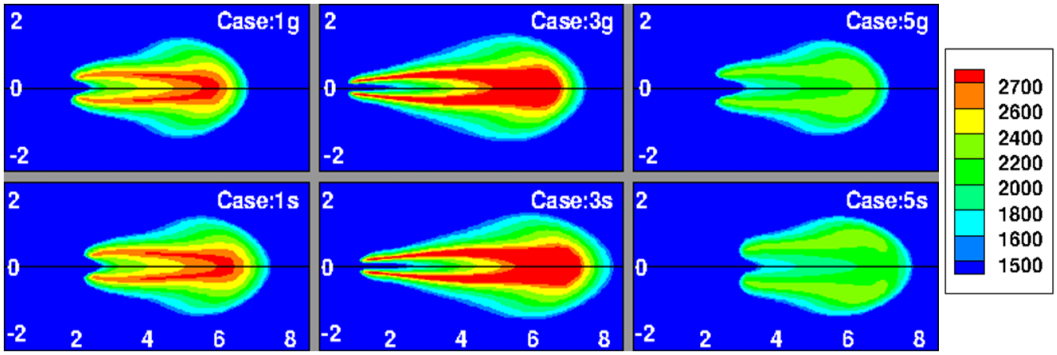

Figure 3. Computed temperature contours for spray and vapor jets at 2.5 ms ASI.

One of the potential strengths of the UFPV model is its ability to predict the transient evolution of reactive scalars in the jet, including during autoignition (and extinction). Figure 4 shows the transient evolution of the temperature contours for Case 1. Note that the temperature range shown is 1500-2700 K. The jet initially penetrates into the chamber without significant rise in temperature. This ignition delay period is affected by the fuel/air mixture ratio and scalar dissipation rate [47]. Higher scalar dissipation rates are associated with higher diffusion rates of the radicals and heat which would then retard ignition. The first significant rise in temperature is observed at 0.55 ms ASI in the rich mixture towards the leading edge of the jet. Subsequent to this, an ignition front propagates into the stoichiometric mixture [50], and then a flame propagates upstream, and stabilizes at the lift-off height at the point where the local scalar dissipation rate is equal to the ignition scalar dissipation rate. Beyond about 1.2 ms (not shown in figure), the front no longer propagates upstream.

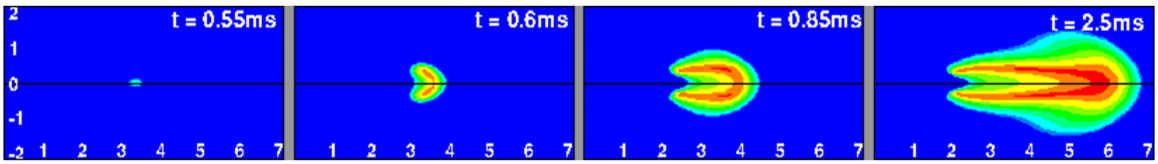

Figure 4. Transient development of temperature contours for the vapor jet.

Figure 5 shows the computed temperature contours for the nine cases, respectively at 2.5 ms ASI when steady lift-off height is achieved in all cases. Quantitative results for the nine cases of Table 2 are presented in Table 3. The measured lift-off height is obtained through measurements of OH chemiluminescence, though, as Ref. [33] discusses, the measurements may also be influenced by other factors such as soot luminosity. In the computations, lift-off will be identified on the basis of temperature and OH mass fraction cut-off values. Absolute cut-off value of 1500 K and 0.001 is employed for temperature and OH mass fraction, respectively. In addition 5% of the total temperature rise and 5% of peak OH mass fraction are also employed as criteria. The measured ignition delay is obtained as the time when the pressure in the chamber shows significant rise as a result of heat release [33]. In the computations, the same temperature cut-off values employed to identify lift-off are employed to identify ignition delay. Using the temperature for the ignition delay is reasonable since it correlates with heat release. The pressure is not a sensitive criterion. The experimental conditions for Case 2 are approximated to be those of a diesel jet injected at 432 K instead of an n-heptane jet injected at 373 K.

It can be seen that when employing T_1500 as a criterion, the differences between computed and measured ignition delay results are within 30% for Cases 1 to 6 and Case 8. Cases 7 and 9 are the ones with lower O_2 concentration. For these two cases, the differences between computed and measured ignition delay results are as large as 50%. Differences between computed and measured lift-off heights, employing the same criterion are within 10 % for all cases except Case 7. Note that Case 7 is the one with lowest O_2 concentration. If 5% temperature rise is considered as a criterion, the differences in ignition delay vary from about 2% for Case 1 to about 30% for Case 5. Case 9 is an outlier in that the difference is about 60%. In the case of lift-off heights, the differ-

ences vary from about 2% in Case 1 to about 12% in Case 4. Notice that the differences are generally smaller than when absolute cut-off values were used. When 5% peak OH is used as a criterion, the differences lie within 25% except for Case 7. Not surprisingly the measure employed to quantify ignition delay and lift-off height influences the results. *Most importantly, however, for all measures considered, the UFPV model predicts the trends (changes) in the ignition delay and flame lift-off accurately for the wide range of conditions considered.*

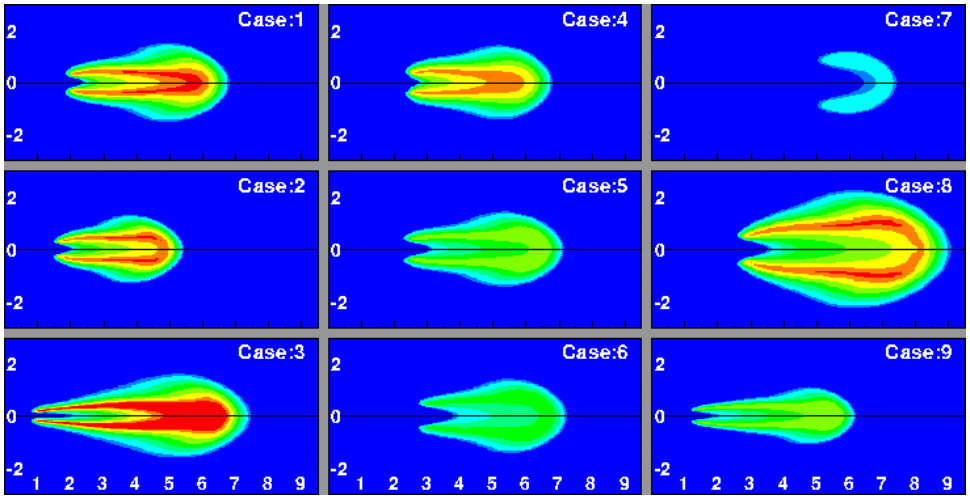

Figure 5. Lift-off height for nine cases of Table1 employing T_1500 criterion.

Table 3 Computed and Measured ignition delay and lift-off height

Case	Ignition Delay τ_{id} (ms)			Lift-off Height L_F (mm)				
	Measured	Computed		Measured	Computed			
		T_1500	T_5%		T_1500	OH_0.001	T_5%	OH_5%
1	0.53	0.542	0.522	17	18.5	18	17.4	17.26
2	-	0.615	0.595	13.5[a]	15.05	14.8	14.33	14.16
3	0.26	0.209	0.205	7.7	8.05	8.25	7.98	8.03
4	0.79	0.89	0.86	25.5	23.3	22.8	22.2	21.88
5	0.73	0.56	0.522	23.2	22.9	22.9	21.6	21.4
6	0.947	1.225	1.275	29.2	27.3	----	25.93	25.37
7	1.52	2.17	1.55	42.3	52.88	----	43.96	45.89
8	0.57	0.65	0.625	23.97	25.8	25.31	24.76	24.21
9	0.38	0.175	0.145	11.9	12	12.8	11.2	11.16

[a] Estimated Value: This value is for diesel fuel injected at 432K

The computed lift-off heights obtained employing the UFPV model correlate with the ignition scalar dissipation rates. The results of Fig. 6 and Table 3 can be understood from this perspective. Case 2 has lower injection pressure which results in lower scalar dissipation rates in the near-field of the jet relative to Case 1 thereby enabling the propagating front to travel farther upstream relative to Case 1. Case 3 has a higher chamber temperature increasing the ignition strain rate of the flame whereas the scalar dissipation rates in the near-field of the jet remain the same as in Case 1. The flame can propagate farther upstream before the ignition scalar dissipation rate is matched by the local scalar dissipation rate. The opposite effect is shown for Case 4 where the chamber temperature is lower. Cases 5-7 and 9 can also be explained in this way. In Case 8, the orifice diameter is increased and the lift-off height increases. Note that the injection velocity in Case 8 is the same as in Case 1. With increasing orifice diameter, the fuel injection rate increases. From scaling laws, it can be shown [51] that the ratio of mass of air entrained to mass injected decreases inversely with increasing diameter. When lesser mass is entrained (in a relative sense), the scalar dissipation rate decreases slower with axial distance. Hence, the ignition scalar dissipation rate is equal to the local scalar dissipation rate at a greater axial distance in the jet.

It is difficult to conclude if the discrepancies noted above are a result of inaccuracies in the UFPV model, the turbulence model, the chemical kinetics mechanism, or the measures used to identify lift-off height and ignition delay – perhaps, it is some combination of all of these. In prior work [47], it has been shown through DNS that the assumption that the scalar dissipation rate can be represented by Eq. (3) and the independent parameters are statistically independent, as discussed earlier, are not generally applicable for reacting diesel jets because of the influence of heat release. Yet, predicted ignition delay and lift-off results show reasonable agreement with

measured results. In the case of ignition delay, an argument can be made that since there is no heat release prior to autoignition, it will not be affected by the errors in the assumptions. Furthermore, after the onset of autoignition, heat release will be accelerated by the decreasing scalar dissipation rate. In the case of lift-off, the explanation is less obvious. One possible explanation is that near and upstream of the lift-off height the scalar dissipation rate is not influenced significantly by the combustion downstream. In fact, Ref. [38] made this assumption in estimating lift-off heights employing scalar dissipation rate values in non-reacting diesel jets. Figure 7 shows the radial variation of the scalar dissipation rate at different axial locations in the jet of Case 1 at 1.5 ms ASI. The axial locations shown are 15, 17, and 20 mm in the jet. Results are shown for reacting and non-reacting jets. Recall that the lift-off height for this case is about 17 mm and this is achieved at about 1.0 ms ASI. Figure 7 (a) shows that the reacting and non-reacting results are almost the same upstream of the lift-off height. Figure 7 (b) shows that at the lift-off height there is a small decrease in the scalar dissipation rate of the reacting jet relative to the non-reacting jet. The differences between the reacting and non-reacting cases become greater at 20 mm downstream (see Fig. 7(c)) where the peak temperature is over 2500 K. It appears from these results that the diffusion of heat upstream is balanced by convection of heat downstream at the lift-off height and the field upstream is not significantly modified. This may explain the reasonable agreement between predicted and measured results, notwithstanding prior finding that the influence of heat release rate on scalar dissipation rate is not captured by the UFPV model.

Summary and Conclusions

Measured fuel distribution, penetration, and spreading of vaporizing diesel sprays injected at high pressure into high-pressure high-temperature chambers can be reproduced with adequate accuracy by a vapor jet model. Lagrangian-drop vaporizing spray models can also predict the measured results with reasonable accuracy if the drop size is carefully selected and the maximum possible grid resolution is employed. Grid independence cannot be, however, ensured. The vapor jet model is employed to evaluate an unsteady flamelet progress variable (UFPV) model to predict autoignition and flame lift-off in RANS simulations of diesel jets over a range of conditions which include changes in injection pressure, ambient temperature, ambient density, and ambient oxygen concentration, and orifice diameter. For the range of conditions considered, ignition delay and flame lift-off heights are generally predicted within 30% of experimental values. Recognizing that these are RANS simulations and there are uncertainties in different aspects of the models employed, including the UFPV model, the most important conclusion is that the simulations reproduce the trends in ignition delay and flame lift-off height accurately for the wide range of conditions. The UFPV model predicts the lift-off height through a mechanism that predicts lift-off is controlled by ignition scalar dissipation rates. It appears that ignition delay and flame lift-off are controlled by processes which are not significantly influenced by the limitations of the UFPV model identified in earlier work. A key shortcoming of the UFPV model is that the effect of heat release on scalar dissipation rates is not taken into account in the model. That the computed and measured results agree within 30 % suggest that the controlling scalar dissipation rates are those which are not affected by the heat release rates.

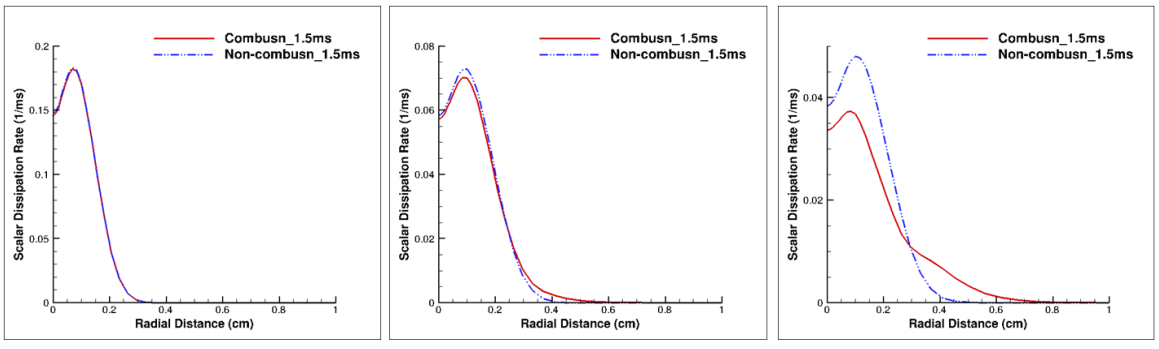

Figure 7. Radial variation of scalar dissipation rate at axial distances of (a) 15 mm, (b) 17 mm, and (c) 20 mm.

Acknowledgements

The authors thank Professor Vinicio Magi for useful discussions related to the implementation of the UFPV model in the RANS code. They authors thank the Rosen Center for Advanced Computing at Purdue University and the National Center for Supercomputing Applications (NCSA) for providing the computing resources for this work. Financial support for this work was provided by Caterpillar, Inc.

References

[1] Siebers, D. L., *SAE paper* 980809 (1998).
[2] Iyer, V., Post, S.L., and Abraham, J., *Proceedings of the Combustion Institute* 28:1111-1118 (2000).
[3] Naber, J., Siebers, D., *SAE Paper* 960034 (1996).
[4] Abraham, J., *SAE Transactions* 106: 141-155 (1997).
[5] Iyer, V.A., Abraham, J., *Combustion Science and Technoogy*. 130: 315–335 (1997).
[6] Post, S., Iyer, V., and Abraham, J., *Journal of Fluids Engineering* 122:385-395 (2000).
[7] Abraham, J., Pickett, L.M., *Atomization and Sprays* 20: 241–250 (2010).
[8] Idicheria, C.A., Pickett, L.M., *SAE Paper 2007-01-0647* (2007).
[9] Bajaj, C., Abraham, J., and Pickett, L., *Atomization and Sprays* 21-5:411–426 (2011).
[10] Abraham, J., and Magi, V., *SAE paper* 1999-01-0911, *SAE Transactions* 3:1363–1374 (1999).
[11] Bracco, F., *SAE Transactions* 94:144-167 (1985).
[12] Reitz, R., *Atomization Spray Technol*ogy 31:309–337 (1987).
[13] O'Rourke, P., and Amsden, A., (1987). *SAE Paper* 872089.
[14] Abraham, J. and Magi, V., *SAE Paper* 970885 (1997).
[15] Iyer, V., Abraham, J., *Journal of Fluids Engineering* 125: 660-669 (2003).
[16] Iyer, V., Abraham, J., *Atomization and Sprays* 15: 249-269 (2005).
[17] Dec, J.E., *SAE Paper* 970873 (1997).
[18] Abraham, J., Williams, F.A., Bracco, F.V., *SAE Paper 850345* 1985
[19] Williams, F.A., *Combustion Theory* 2nd Edition, Westview Press (1985).
[20] Peters, N., *Turbulent Combustion*, Cambridge University Press, Cambridge, UK, 2000.
[21] Peters, N., *Progress in Energy and Combustion Science* 10:319-339 (1984).
[22] Williams, F.A., (1985). *Turbulent Combustion*, in J.Buckmaster, editor, The Mathematics of Combustion, 97-131, SIAM, Philadelphia.
[23] Klimenko, A.Y., and Bilger, R.W., *Progress in Energy and Combustion Science* 25-6:25-62 (1999).
[24] Pitsch, H., *Annual Review of Fluid Mechanics* 38:453-483 (2006).
[25] Abraham, J., and Bracco, F., *SAE Paper* 932656 (1993).
[26] Kong, S., Han, Z., and Reitz, R.D., *SAE Paper*, 950278 (1995).
[27] Chomiak, J., Karlsson, A., *Proceedings of the Combustion Institute* 26: 2557-2564 (1996).
[28] Sazhina, E. M., Sazhina, S. S., Heikal, M.R., Babushok, V.I., and Johns, R.J.R., *Combustion Science and Technology*, 160-1:317-344 (2000).
[29] Tao, F., Chomiak, J., *SAE Paper* 2002-01-1114 (2002).
[30] Senecal, P.K., Pomraning, E., Richards, K.J., Briggs, T.E., Choi, C.Y., McDavid, R.M., and Patterson, M.A., *SAE Paper* 2003-01-1043 (2003).
[31] Venugopal, R., Abraham, J., *SAE Paper* 2007-01-0134 (2007).
[32] Karrholm, F.P., Tao, F., Nordin, N., *SAE Paper* 2008-01-0961 (2008).
[33] Siebers, D.L., Higgins, B., *SAE Paper* 2001-01-0530 (2001).
[34] Pitts, W.M., *Proceedings of the Combustion Institute* 22:809- 816 (1988).
[35] Lyons, K. M., *Progress in Energy and Combustion Science* 33: 211-231 (2007).
[36] Lawn, C. J., *Progress in Energy and Combustion Science* 35:1-30 (2009).
[37] Tap, F.A., Veynante, D., *Proceedings of the Combustion Institute* 30: 919-926 (2005).
[38] Venugopal, R., Abraham, J., *Combustion Science and Technology* 179: 2599-2618 (2007).
[39] Pitsch, H., Wan, Y.P., and Peters, N., *SAE Paper* 952357 (1995)..
[40] Errico, G.D., Ettorre, D., and Lucchini, T., *SAE International* 2008-01-0954 (2008).
[41] Pickett, L.M., Siebers, D.L., and Idicheria, C.A., *SAE Paper* 2005-01-3843 (2005).
[42] Magi, V., Iyer, V., and Abraham, J., *Numerical Heat Transfer* A40:317-334 (2001).
[43] Wilcox, D. C., *Turbulence Modeling for CFD*, La Canada, CA: DCW Industries, Inc., chap. 4.
[44] Pope, S., *AIAA Journal*, 6:279-281 (1978).
[45] Pitsch, H., Ihme, M., *AIAA Paper* 2005-557 (2005).
[46] Ihme, M., See, Y.C., *Combustion and Flame* 157: 1850-1862 (2010).
[47] Mukhopadhyay, S., *Ignition and Early Flame Development in Stratified-Charge Mixtures*, PhD thesis, Purdue University, West Lafayette, IN, USA, August 2011.
[48] Pitsch, H., Barths, H., and Peters, N., *SAE Paper* 962057 (1996).
[49] Liu, S., Hewson, J.C., Chen, J.H., and Pitsch, H., *Combustion and Flame* 137: 320-339 (2004).
[50] Mukhopadhyay, S., Abraham, J., *Combustion and Flame* 158: 1064-1075 (2011).
[51] Abraham, J., *Numerical Heat Transfer* 30-4:347–364 (1996).